Biophysical Chemistry 159 (2011) 58–65

Contents lists available at ScienceDirect

Biophysical Chemistry

journal homepage: http://www.elsevier.com/locate/biophyschem

Equilibrium and kinetic studies of protein cooperativity using urea-induced folding/unfolding of a Ubq–UIM fusion protein

Mayank M. Patel, Franco Tzul, George I. Makhatadze *

Center for Biotechnology and Interdisciplinary Studies, Rensselaer Polytechnic Institute, 110 8th Street, Troy, NY 12065, USA
Department of Biology, Rensselaer Polytechnic Institute, 110 8th Street, Troy, NY 12065, USA

ARTICLE INFO

Article history:
Received 11 April 2011
Received in revised form 3 May 2011
Accepted 3 May 2011
Available online 13 May 2011

Keywords:
Protein cooperativity
Protein stability
Protein engineering

ABSTRACT

Understanding the origins of cooperativity in proteins remains an important topic in protein folding. This study describes experimental folding/unfolding equilibrium and kinetic studies of the engineered protein Ubq–UIM, consisting of ubiquitin (Ubq) fused to the sequence of the ubiquitin interacting motif (UIM) via a short linker. Urea-induced folding/unfolding profiles of Ubq–UIM were monitored by far-UV circular dichroism and fluorescence spectroscopies and compared to those of the isolated Ubq domain. It was found that the equilibrium data for Ubq–UIM is inconsistent with a two-state model. Analysis of the kinetics of folding shows similarity in the folding transition state ensemble between Ubq and Ubq–UIM, suggesting that formation of Ubq domain is independent of UIM. The major contribution to the stabilization of Ubq–UIM, relative to Ubq, was found to be in the rates of unfolding. Moreover, it was found that the kinetic m-values for Ubq–UIM unfolding, monitored by different probes (far-UV circular dichroism and fluorescence spectroscopies), are different; thereby, further supporting deviations from a two-state behavior. A thermodynamic linkage model that involves four states was found to be applicable to the urea-induced unfolding of Ubq–UIM, which is in agreement with the previous temperature-induced unfolding study. The applicability of the model was further supported by site-directed variants of Ubq–UIM that have altered stabilities of Ubq/UIM interface and/or stabilities of individual Ubq- and UIM-domains. All variants show increased cooperativity and one variant, E43N_Ubq–UIM, appears to behave very close to an equilibrium two-state.

1. Introduction

One of us (GIM) has been participating in the Gibbs conference since 1991, first as a freshly minted postdoc and then as a PI. Gibbs played a vital role in my development as a scientist and as a member of the Biothermodynamics community. I have met many people at Gibbs who have influenced my career (John Schellman, Buzz Baldwin, Nick Pace, Wayne Bolen, Clare Woodward, George Rose, Rod Biltonen, and Jim Lee) and I have met wonderful colleagues who since became my friends (Dorothy Beckett, Michael Henzl, Bertrand Garcia-Moreno, Karen Fleming, Trevor Creamer, Louis Marky, Doug Barrick, and Rohit Pappu to name a few). There are also these wonderful personalities—Jack Correia, Mike Johnson and Tim Lohman—that make this meeting such fun. It is a wonderful meeting of scientists working on advancing the understanding of biology from thermodynamic principles, as well as a great educational forum for graduate students and postdocs. Happy 25th anniversary Gibbs!

One of the most important take-home messages that a newcomer learns at Gibbs is the notion of thermodynamic linkage. This linkage theory, summarized most recently by Wyman and Gill [1] and DiCera [2], provides detailed understanding of such complex processes as binding, folding, and conformational transition. In this paper, we used thermodynamic linkage for the analysis of thermodynamic basis of cooperativity for the engineered model system, Ubq–UIM fusion.

The problem of protein cooperativity is one of the central problems in protein folding. It has been the subject of numerous studies: experimental, computational and theoretical. Several recent experimental studies are particularly noteworthy. Barrick et al. [3–5] have analyzed the folding of ankyrin repeat protein and using the Ising type model have shown that the strength of interaction between individual repeats is the major source of cooperativity in this model system. DeVries et al. [6] used another ankyrin repeat protein and showed that while the protein appears to have an equilibrium folding/unfolding mechanism, it exhibits a non-two-state folding kinetics. Batey et al. [7–9] studied a model protein consisting of two spectrin domains. They have shown, using site-directed amino acid substitutions, that the inter-relation between the stability of individual domains and the stability of the linker region controls the overall cooperativity of the system. Furthermore, they have demonstrated that even though the system behaves as two-state under equilibrium conditions, it

* Corresponding author at: Center for Biotechnology and Interdisciplinary Studies, Rensselaer Polytechnic Institute, 110 8th Street, Troy, NY 12180, USA. Tel.: +1 518 276 4417; fax: +1 518 276 2955.
E-mail address: makhag@rpi.edu (G.I. Makhatadze).

0301-4622/$ – see front matter © 2011 Elsevier B.V. All rights reserved.
doi:10.1016/j.bpc.2011.05.004

shows non-two state kinetics. All these model proteins are naturally occurring and thus it is not always straightforward how to identify the domain boundaries and thus, to dissect the contribution of stabilities of individual domains into the overall energetics.

We have previously engineered a Ubq–UIM fusion protein that allows independent experimental manipulations of the individual domains. It takes advantage of the fact that the ubiquitin interacting motif (UIM), consisting of a 20-residue helix, binds to ubiquitin (Ubq) in an orientation that positions the C-terminus of Ubq in close proximity to the N-terminus of the UIM. Thus, we used a short glycine-based linker to fuse Ubq to UIM [10]. The solution structure of the Ubq–UIM fusion protein (Fig. 1) showed that the structure is very similar to the structure of the non-covalent Ubq/UIM complex [11]. Thermodynamic studies of cooperativity upon temperature-induced unfolding of Ubq–UIM showed that it does not follow two-state unfolding but includes detectable population of two equilibrium intermediate states consisting of either one of the two domains (Ubq or UIM) folded and the other unfolded. This model was further supported by the studies of the Ubq–UIM variants with altered stabilities of individual domains (Ubq or UIM) or domain–domain (Ubq/UIM) interface. Furthermore, molecular dynamics simulations using the Ubq–UIM solution structure also supported the presence of these intermediates [10].

In this paper, we extend the analysis of cooperativity of the Ubq–UIM protein to urea-induced unfolding using equilibrium and kinetic experiments. This is important because temperature and urea are very dissimilar denaturing agents and may modulate the equilibrium and kinetic populations of the intermediate states differently. Using far-UV circular dichroism spectroscopy to monitor changes in the secondary structure of both Ubq and UIM domains and fluorescence spectroscopy to monitor specifically the changes in the structure of the Ubq domain, we were able to show that the Ubq–UIM folding/unfolding reaction is not a two-state process. We have characterized the transition state ensemble for folding of Ubq–UIM and have shown that it is very similar to the folding transition state ensemble of Ubq. Overall, the stabilization of Ubq–UIM occurs due to the decrease in the unfolding rates of the protein. Multistate thermodynamic and kinetic models of Ubq–UIM unfolding are further supported by the site-directed variants of Ubq–UIM.

2. Materials and methods

2.1. Cloning, expression and purification

The expression and purification of Ubq and Ubq–UIM proteins has been described in details elsewhere [10]. Purity and identity of the recombinant proteins were confirmed by MALDI TOF mass spectroscopy.

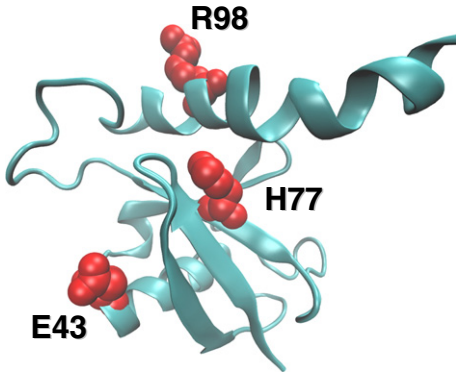

Fig. 1. Cartoon structure of Ubq–UIM drawn using PDB entry (1KDI) with side chains at the position of single amino acid substitutions shown in CPK presentation. Figure is drawn using VMD [34].

Protein concentrations were determined spectrophotometrically using extinction coefficients of $\varepsilon_{280nm} = 6990\ M^{-1}\ cm^{-1}$ for Ubq variants, and $\varepsilon_{280nm} = 8480\ M^{-1}\ cm^{-1}$ for Ubq–UIM variants [12].

A previous study in our laboratory has established that the Ubq–UIM fusion construct, under the experimental conditions used here, is monomeric in solution, [10]. Furthermore, no dependence of relaxation kinetics on protein concentration was observed.

2.2. Circular dichroism spectroscopy

CD experiments were carried out on a JASCO J-715 spectropolarimeter. Far-UV spectra were acquired in triplicate in 1 mm quartz cylindrical cuvettes at concentrations of ~0.3 mg/ml. All experiments were carried out in CD buffer containing 1 mM each of sodium borate, sodium citrate, and sodium phosphate [13].

Urea-induced denaturation curves were determined from wavelength scans of Ubq and Ubq–UIM in a 1 cm rectangular cuvette as a function of urea concentration, which was controlled by a JASCO dual syringe auto-titrator. The protein stock solutions were prepared by dialysis into water at concentrations ~5 mg/ml. Final samples were prepared by diluting appropriate volumes of stock solution into CD buffer (described above) pre-adjusted to pH 7.4 to obtain protein concentrations ~35 μg/ml. This dilution factor is so large that the buffer pH is not detectably changed. Urea stock solutions were freshly prepared in CD buffer and final urea concentrations were measured using refractive index [14].

2.3. Fluorescence spectroscopy

Steady-state fluorescence experiments were performed on a FluoroMax spectrofluorimeter with DM3000F software (SPEX Industries, Inc.). A constant temperature (25 °C) in the thermostated cell holder was maintained using a Neslab automated circulating water-bath. Fluorescence emission spectra were recorded from 310–500 nm in a 1 cm rectangular quartz cuvette using an excitation wavelength of 295 nm, step resolution of 0.5 nm, an integration time of 3 s, and excitation and emission slit widths of 2 and 7 nm, respectively.

For urea titrations, the same excitation wavelength was used. Sample preparation concentrations, buffer conditions and data analysis are the same as described for urea titrations monitored by CD as described above, except that aliquots of stock buffered urea solution were added to the cuvette using a Hamilton dual syringe auto-titrator [15]. Denaturation profiles were obtained by plotting emission intensity at 354 nm as a function of urea concentration.

2.4. Equilibrium data analysis

The analysis of urea unfolding curves was carried out by implementing the linear extrapolation method assuming a two-state unfolding transition [16] into the non-linear regression routine NLREG. Briefly, the denaturation curves were fitted to the following equation:

$$Y([urea]) = F_N([urea])\cdot Y_N([urea]) + F_U([urea])\cdot Y_U([urea]) \quad (1)$$

where Y([urea]) is the measured fluorescence intensity at 354 nm or ellipticity at 222 nm at a urea concentration [urea], Y_N([urea]) and Y_U([urea]) are fluorescence intensity or ellipticity values of the native and unfolded protein, respectively, F_N([urea]) and F_U([urea]) are fractions of the native and unfolded protein at this urea concentration. The fractions of the native and unfolded proteins were calculated as

$$F_N([\text{urea}]) = 1 - F_U([\text{urea}]) = \frac{1}{1 + K([\text{urea}])} \quad (2)$$

where $K([\text{urea}])$ is the equilibrium constant of the two-state unfolding reaction at different urea concentrations, calculated as

$$K([\text{urea}]) = \exp\left(-\frac{\Delta G([\text{urea}])}{RT}\right) \quad (3)$$

where, $\Delta G([\text{urea}])$ is the free energy of unfolding, which is assumed to be a linear function of denaturant concentration, and is determined from the following equation:

$$\Delta G([\text{urea}]) = \Delta G_{eq}^{H_2O} - m\cdot[\text{urea}] \quad (4)$$

where [urea] is the urea concentration in molar units, $\Delta G([\text{urea}])$ and $\Delta G_{eq}^{H_2O}$ are the Gibbs free energies for protein unfolding at a given [urea], and that in the absence of urea, respectively.

2.5. Stopped flow circular dichroism and fluorescence

Stopped flow CD and fluorescence experiments were performed on a JASCO J-815 spectropolarimeter equipped with an SFM 300 mixing module (BioLogic Science Instruments). Kinetic traces were obtained by monitoring the ellipticity at 222 nm or the fluorescence emission intensity after excitation at 295 nm using a 320 nm cutoff filter. Protein samples were dialyzed against two changes of 1 l each of CD buffer, pH 7.4. For the refolding experiments, unfolded protein samples (~3 mg/ml) containing 9 M urea in CD buffer were diluted eleven-fold with refolding CD buffer, pH 7.4, and the appropriate amounts of 8 M urea solution to achieve final urea concentrations in the range from 0.5 M to 4 M for Ubq and 6.5 M for Ubq–UIM. The stock solution for unfolding experiments contained ~3 mg/ml protein in CD buffer. Unfolding reactions were initiated by mixing the stock protein solution with appropriate volumes of CD buffer and 9.5 M urea in buffer. The measurements were conducted at 25 °C, controlled by a circulating water-bath.

2.6. Kinetic data analysis

Kinetic traces were analyzed using the Bio-Kine32 software provided with the instrument to determine folding and unfolding rate constants at various urea concentrations. The "chevron analysis" was used to fit the urea dependence of folding and unfolding rate constants using the following equation [17–19]:

$$\ln(k_{obs}([urea])) = \ln\left[\exp\left(\ln(k_f) + \frac{m_f[urea]}{RT}\right) + \exp\left(\ln(k_u) + \frac{m_u[urea]}{RT}\right)\right] \quad (5)$$

where $k_{obs}([\text{urea}])$ is the observed rate constant at urea concentration [urea], k_f and k_u are the folding and unfolding rate constants, respectively, extrapolated to zero denaturant concentration, and m_f and m_u are the kinetic m-values and represent the slopes of the two arms of the chevron plot. The Gibbs free energy of folding from kinetic experiments was calculated as

$$\Delta G_{kin}^{H_2O} = -R\cdot T\cdot \ln\left(\frac{k_f}{k_u}\right) \quad (6)$$

where $\Delta G_{kin}^{H_2O}$ is the Gibbs free energy of unfolding at zero denaturant concentration.

3. Results and discussion

3.1. Equilibrium stability of Ubq–UIM: evidence for deviation from 2-state unfolding

The major goal of this study is to examine whether the Ubq–UIM fusion protein exhibits two-state or multi-state behavior upon urea-induced unfolding. This has been done by comparing the urea-induced unfolding profiles of Ubq and Ubq–UIM monitored by changes in far-UV CD at 222 nm and by changes in fluorescence emission intensity at 354 nm following Trp54 excitation at 295 nm. The use of multiple spectroscopic techniques to study protein folding cooperativity is well established [20–23], and it is based on the ability of these techniques to monitor changes in protein structure at different levels. Far-UV CD at 222 nm monitors the secondary structure content in proteins and is most sensitive to helical context. In Ubq–UIM, the far-UV CD signal at 222 nm is dominated by the UIM helix, although the 10-residue helix in Ubq also contributes to this signal, meaning that this technique provides information on the helical content of Ubq–UIM [10]. On the other hand, changes in the fluorescence signal are due to changes in polarity of the environment around aromatic amino acids, and thus monitor tertiary structure in proteins. In Ubq–UIM we have monitored the fluorescence emission intensity of the only Trp residue (introduced by the F54W substitution), which is able to monitor changes in tertiary structure of the fusion construct [24]. A convergence of the unfolding profiles followed by these two different techniques would suggest a cooperative unfolding behavior, and vice versa.

The urea-induced unfolding profiles of Ubq and Ubq–UIM monitored by CD and fluorescence are shown in Fig. 2 and exhibit a single sigmoidal transition. Both techniques show that Ubq–UIM is more stable than Ubq: the midpoint of the unfolding transition ($C_{1/2}$) for Ubq–UIM is higher than that of Ubq by ~2 M. The unfolding profiles for Ubq, monitored by both techniques, overlap, which is consistent with the established two-state unfolding behavior of Ubq [24,25]. Furthermore, these profiles could be fit to a two-state unfolding model with essentially the same thermodynamic parameters, $\Delta G_{eq}^{H_2O}$ and m-value (Table 1).

However, the unfolding profiles for Ubq–UIM monitored by CD and fluorescence clearly do not overlap and could not be globally fitted to a two-state unfolding model. Results from individual fits yield different Gibbs free energies of unfolding ($\Delta G_{eq}^{H_2O}$) from CD- and fluorescence-monitored unfolding: $\Delta G_{eq,CD}^{H_2O}$ is ~6 kJ/mol higher than $\Delta G_{eq,FL}^{H_2O}$ (Table 1). A closer look at the fitted parameters for Ubq–UIM shows that this difference predominantly arises from differences in the m-values, i.e., the urea dependence of ΔG given by the slope of the transition region in equilibrium unfolding curves. Specifically, m_{FL} (4.3 ± 0.1 kJ mol^{-1} M^{-1}) is lower than m_{CD} (5.1 ± 0.1 kJ mol^{-1} M^{-1}). Interestingly, m_{FL} for Ubq–UIM is similar to the m-value of Ubq ($m = 4.2 \pm 0.2$ kJ mol^{-1} M^{-1}).

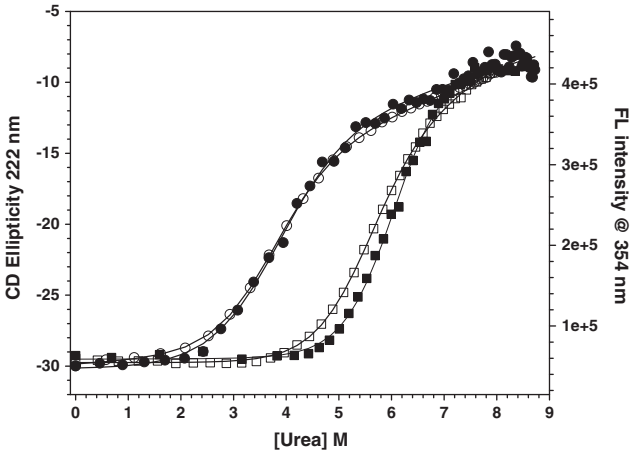

Fig. 2. Urea-induced equilibrium unfolding curves of Ubq (circles) and Ubq–UIM fusion protein (squares) monitored by far-UV CD ellipticity monitored at 222 nm (filled symbols) and fluorescence intensity at an emission wavelength of 354 nm (excitation at 295 nm) (open symbols). Solid lines indicate fits to a two-state unfolding model with the parameters given in Table 1.

Table 1
Equilibrium thermodynamic parameters for Ubq and Ubq–UIM variants.

Approach	Protein	Method	[a]$\Delta G_{eq}^{H_2O}$ (kJ/mol)	[b]m_{eq} (kJ mol^{-1}·M^{-1})
Equilibrium	Ubq	[c]CD&FL	16.0 ± 1.2	4.2 ± 0.2
	Ubq–UIM	CD	30.8 ± 1.2	5.1 ± 0.1
		FL	24.6 ± 1.1	4.3 ± 0.1
	H77V_Ubq	[c]CD&FL	17.7 ± 1.7	4.3 ± 0.2
	H77V_Ubq–UIM	CD	37.7 ± 2.0	5.4 ± 0.2
		FL	30.9 ± 1.2	4.4 ± 0.1
	E43N_Ubq	FL	8.2 ± 1.5	4.0 ± 0.1
	E43N_Ubq–UIM	CD	24.5 ± 2.0	5.4 ± 0.2
		FL	23.0 ± 1.0	5.0 ± 0.1
	R98V_Ubq–UIM	CD	28.6 ± 1.1	5.4 ± 0.1
		FL	22.5 ± 0.9	4.3 ± 0.1
			$\Delta G_{kin}^{H_2O}$ (kJ/mol)	m_{kin} (kJ mol^{-1}·M^{-1})
Kinetic	Ubq	[c]CD&FL	16.2 ± 1.1	4.2 ± 0.2
	Ubq–UIM	CD	30.3 ± 1.1	5.2 ± 0.2
		FL	25.0 ± 1.3	4.3 ± 0.2
	H77V_Ubq	FL	18.5 ± 0.8	4.1 ± 0.2
	H77V_Ubq–UIM	CD	35.1 ± 1.2	4.9 ± 0.2
		FL	29.0 ± 1.1	4.1 ± 0.2
	E43N_Ubq	FL	10.0 ± 0.7	4.2 ± 0.2
	E43N_Ubq–UIM	CD	22.2 ± 1.0	5.1 ± 0.2
		FL	21.7 ± 0.8	5.0 ± 0.2
	R98V_Ubq–UIM	CD	22.9 ± 0.9	5.0 ± 0.2
		FL	21.3 ± 1.1	4.7 ± 0.2

[a] Gibbs free energy of unfolding determined by fitting urea-induced unfolding profiles (Fig. 2) to Eqs.(1) – (4) for equilibrium, and urea dependence of folding and unfolding rate constants (Fig. 5) to Eq.(5) for kinetic experiments, respectively.
[b] Urea dependence of the Gibbs free energy of unfolding determined from Eq. (4) for equilibrium unfolding. The *m*-values for kinetic experiments are calculated as $m_u - m_f$ (see Table 2) for comparison with equilibrium *m*-values.
[c] Parameters from global fits of unfolding curves monitored by far-UV CD and fluorescence spectroscopies.

The obtained m-values of Ubq and Ubq–UIM are consistent with structure-based calculations. The accepted interpretation of the m-value is that it provides a measure of changes in total solvent accessible surface area (ΔASA) upon urea-induced unfolding. Pace et al. have derived an empirical relationship between m-value and ΔASA [26]:

$$m\left(kJ\cdot mol^{-1}\cdot M^{-1}\right) = 1.56 + 4.6\cdot 10^{-4}(\Delta ASA) \quad (7)$$

We have used this equation to calculate the expected m-values for Ubq and Ubq–UIM using the structure of Ubq–UIM we have solved recently (PDB entry 2KDI [11]). The unfolded state structure was modeled as an extended chain with the respective amino acid sequence. Calculations show that the ΔASA values are 5500 Å^2 for Ubq and 7550 Å^2 for Ubq–UIM. Using these ΔASA, the *m*-values obtained for Ubq and Ubq–UIM from Eq. (7) are 4.1 and 5.0 kJ·mol^{-1}·M^{-1}, respectively. Thus, the structure-based estimates of the m-value for Ubq are in very good agreement with the values obtained experimentally from urea-induced unfolding experiments using either fluorescence or far-UV CD (Table 1). The structure-based estimate of the m-value for Ubq–UIM is in agreement with the experimental m-value obtained from unfolding experiments monitored using far-UV CD. Importantly, the experimental m-value for Ubq–UIM obtained from the unfolding monitored by fluorescence is similar to that of Ubq. Recall that changes in fluorescence exclusively monitor changes in tertiary structure, i.e., unfolding of the Ubq core, while changes in far-UV CD monitor the unfolding of both Ubq core and UIM. This suggests that the changes in fluorescence reflect the unfolding of Ubq core in Ubq–UIM, while the changes in far-UV CD reflect the unfolding of the entire Ubq–UIM molecule, and these two do not overlap.

3.2. Test of equilibrium unfolding model by selective modulation of stabilities of Ubq core, UIM helix or Ubq/UIM interface via site-directed substitutions

We have previously established that a four state equilibrium thermodynamic model adequately describes the temperature-induced unfolding of Ubq–UIM [10]. The same model (Fig. 3) can be adopted to describe the thermodynamic linkage between different states in the presence of urea. The populations of different states that describe the equilibrium four state unfolding of Ubq–UIM are defined by the partition function Q as:

$$Q = 1 + K_{int}\cdot K_{Ubq} + K_{int}\cdot K_{UIM} + K_{int}\cdot K_{Ubq}\cdot K_{UIM} \quad (8)$$

where K_{ubq}, K_{UIM} and K_{int}, represent the equilibrium constants in the absence of denaturant for unfolding of Ubq domain, UIM helix, and Ubq/UIM interface, respectively. These equilibrium constants depend on urea concentration (assuming the validity of linear extrapolation model) as:

$$K_{Ubq}[urea] = \exp\left(-\frac{\Delta G_{Ubq,H_2O} - m_{Ubq}\cdot[urea]}{RT}\right) \quad (9)$$

$$K_{UIM}[urea] = \exp\left(-\frac{\Delta G_{UIM,H_2O} - m_{UIM}\cdot[urea]}{RT}\right) \quad (10)$$

$$K_{int}[urea] = \exp\left(\frac{-\Delta G_{int,H_2O} - m_{int}\cdot[urea]}{RT}\right) \quad (11)$$

The populations of individual species are defined as:

$$f_N = 1/Q \quad (12)$$

$$f_I = (K_{int}\cdot K_{UIM})/Q \quad (13)$$

$$f_{II} = \left(K_{int}\cdot K_{Ubq}\right)/Q \quad (14)$$

$$f_U = \left(K_{int}\cdot K_{Ubq}\cdot K_{UIM}\right)/Q \quad (15)$$

The total fractional population as detected by either CD or FL can be calculated by adding the relevant fractional populations from the four states, as follows:

$$f_{FL} = f_N + f_{II} \quad (16)$$

$$f_{CD} = f_N + f_I\cdot\phi_{UIM} + f_{II}\cdot\phi_{Ubq} \quad (17)$$

where ϕ_{Ubq} and ϕ_{UIM} are fractional changes in ellipticity associated with unfolding of the Ubq core and the UIM helix. Unfortunately, direct modeling using experimental data for individual domains is not possible. There are two major obstacles. First, the dependencies of ellipticity for fully helical and fully coiled states are not well established, as opposed to these dependencies on temperature [27,28]. Correspondingly, even having the ellipticity data for the UIM peptide as a function of urea concentration, one cannot calculate the fraction of helical content and correspondingly cannot obtain the dependence of K_{UIM} on urea. Second, the dependence of K_{int} on urea concentration (i.e. m-value) is also difficult to estimate. Considering that the interface is largely formed by side-chain to side-chain interactions, and that urea appears to directly interact with the protein backbone [29,30], the m-value calculated using the empirically derived structure-based Eq. (7) will most probably lead to an overestimate. An alternative approach, a direct fit of the data to the model (Eqs.(8)–(17)) did not show robust convergence, probably due to the fact that the system is underdetermined.

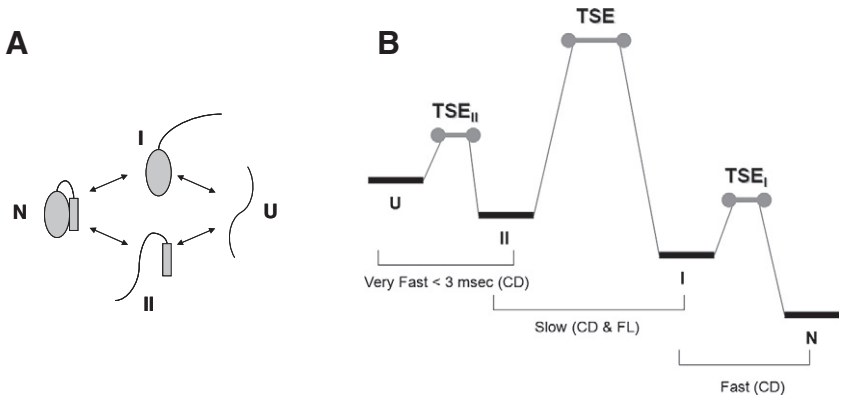

Fig. 3. Equilibrium (panel A) and kinetic (panel B) models for folding/unfolding of Ubq–UIM.

Thus, to further validate the unfolding model for Ubq–UIM, we used amino acid substitutions in Ubq–UIM. The unfolding cooperativity of Ubq–UIM, according to a four state thermodynamic model is described by the magnitude of the Gibbs free energy of Ubq/UIM binding interface relative to the Gibbs free energies of individual domains Ubq core and UIM helix, and by their dependencies of urea concentration. Three single-site substitutions modulating these parameters were made to test the folding cooperativity of Ubq–UIM in the framework of this model (Fig. 1): i) H77V substitution in Ubq domain is located at Ubq/UIM interface and increases both ΔG_{Ubq} and ΔG_{int}; ii) R98V substitution is UIM is located on the opposite side from Ubq binding interface and leads to a decrease in ΔG_{UIM}; and iii) E43N substitution in Ubq domain is located on the opposite side from UIM binding interface and leads to a decrease in ΔG_{Ubq} [31].

Urea-induced equilibrium unfolding profiles of the Ubq–UIM variants H77V_UbqUIM, E43N_Ubq–UIM, and R98V_Ubq–UIM, monitored by CD and fluorescence are shown in Fig. 4, and thermodynamic parameters from a two-state fit are given in Table 1. The differences in the unfolding transitions for these variants, as monitored by these two methods, are dramatically different from that of wild type Ubq–UIM. In all cases, the unfolding profiles monitored by CD or fluorescence are much closer to each other. Yet, the difference exists, suggesting that the unfolding for all these variants is more cooperative than for the wild type but still not two-state.

i. H77V_Ubq–UIM is more stable than Ubq–UIM, independent of technique used to monitor the urea-induced equilibrium unfolding, (Fig. 4 and Table 1). This is consistent with an increase in the stability of Ubq domain (higher ΔG_{ubq}) and stabilized Ubq/UIM interface (higher ΔG_{int}). The unfolding profiles of this variant exhibit similar $C_{1/2}$ values as determined by both CD and fluorescence (Fig. 4), however, fluorescence-monitored unfolding yields a lower thermodynamic stability owing to a lower $m_{eq,FL}$-value (Fig. 4 and Table 1). A stabilized interface in H77V_Ubq–UIM, i.e., higher ΔG_{int}, is expected to increase cooperativity of this variant relative to the wild type Ubq–UIM. Indeed, this is supported by the observation that the unfolding profiles monitored by CD and fluorescence are much closer to each other for H77V_Ubq–UIM than for the wild type Ubq–UIM. (Fig. 4). Nevertheless, H77V_Ubq–UIM unfolding deviates from two-state, i.e. remains non-cooperative.

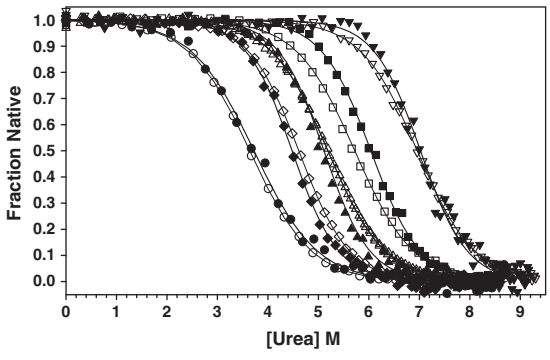

Fig. 4. Fraction of native state as a function of denaturant concentration for urea-induced equilibrium unfolding curves of Ubq (circles) and Ubq–UIM variants (wild type Ubq–UIM—squares; H77V_Ubq–UIM—down triangles; R98V_Ubq–UIM—up triangles; E43N-Ubq–UIM—diamonds) monitored by far-UV CD ellipticity monitored at 222 nm (filled symbols) and fluorescence intensity at an emission wavelength of 354 nm (excitation at 295 nm) (open symbols). Solid lines indicate fits to a two-state unfolding model with the parameters listed in Table 1.

ii. The destabilized UIM helix in the R98V_Ubq–UIM variant, i.e., lower ΔG_{UIM} is expected to lower the stability of the fusion protein due to lower helix propensity of Val relative to Arg [13]. Similar to the H77V_Ubq–UIM and E34N_Ubq–UIM (see below) variants, the $C_{1/2}$ values determined from CD and fluorescence-monitored unfolding profiles are very similar for the R98V_Ubq–UIM variant. The difference in the apparent $\Delta G_{eq}^{H_2O}$ between the two techniques arises due to a larger $m_{eq,CD}$-value (Table 1). Since this substitution does not alter ΔG_{int}, the decrease in ΔG_{UIM} should lead to an increase in the unfolding cooperativity relative to the wild type Ubq–UIM. This is supported by a much smaller difference in the unfolding profiles monitored by CD and fluorescence for R98V_Ubq–UIM (Fig. 4). Nevertheless, a difference in the m-values from CD and fluorescence remains similar to that of wild type Ubq–UIM (Table 1), providing further support that the transitions are not two-state.

iii. Destabilization of the Ubq core (lower ΔG_{Ubq}) by the E43N substitution is reflected in a lower $\Delta G_{eq}^{H_2O}$ of E43N_Ubq–UIM than for the wild type Ubq–UIM as monitored by either CD or fluorescence (Fig. 4 and Table 1). A lower ΔG_{Ubq} with ΔG_{int} unchanged predicts that the E43N_Ubq–UIM variant should be more cooperative than that of Ubq–UIM. This is consistent with the observation that CD and fluorescence unfolding profiles are much closer to each other than to any other variants. Furthermore, the m-values and $\Delta G_{eq}^{H_2O}$ are very similar ($m_{u,FL} = 5.0 \pm 0.1$ kJ mol^{-1} M^{-1} vs. $m_{u,CD} = 5.4 \pm 0.2$ kJ mol^{-1} M^{-1} and $\Delta G_{eq,FL}^{H_2O} = 23.0 \pm 1.0$ kJ/mol vs. $\Delta G_{eq,CD}^{H_2O} = 24.5 \pm 2.0$ kJ/mol). This is consistent with the expected outcome that unfolding of the E43N variant is much more cooperative than the wild type Ubq–UIM and very close to an equilibrium two-state.

The results of thermodynamic analysis on these three variants of Ubq–UIM support a four state unfolding model, and show that when

an appropriate balance of Gibbs free energy is achieved, a cooperative unfolding (i.e. close to two-state as in E43N_Ubq–UIM) can be observed. This finding is consistent with our previous study in which we have shown that during temperature-induced unfolding, significant population of equilibrium intermediates are also populated [10]. We have also shown using MD simulations of the wild type Ubq–UIM that during the temperature-induced unfolding, four different states can be observed: in addition to the native and unfolded states, states that have either Ubq core or UIM helix folded can be populated [10]. We further analyzed this model by experimentally determining the rates of folding/unfolding reaction of Ubq–UIM and compared it to the rates of folding/unfolding reaction of Ubq.

3.3. Kinetic stability of Ubq–UIM—different unfolding rates account for discrepancy in ΔG_{eq} from CD and fluorescence

Equilibrium unfolding data show that urea-induced unfolding of Ubq closely follows a two-state model, while Ubq–UIM shows significant deviation from two-state behavior. Would these trends be preserved in the kinetics of folding/unfolding reactions? What is the effect of Ubq/UIM interactions on the rates of Ubq–UIM folding? To answer these questions folding and unfolding stopped flow kinetics of both proteins were studied by the same methods as were used for the equilibrium studies, far-UV CD and fluorescence spectroscopies.

All kinetic traces exhibit a single phase and could be well described by a single exponential fit. The rate constants show a linear dependence on urea concentration and the resulting chevron plots are shown in Fig. 5. For Ubq, the Gibbs energy ($\Delta G^{H_2O}_{kin}$, see Eq. (6)) and m-value ($m_{eq} = m_u - m_f$) determined from the fit of kinetic CD and fluorescence data to a two-state unfolding model are in very good experiment with the thermodynamic parameters obtained from equilibrium unfolding experiments ($\Delta G^{H_2O}_{eq}$, Table 1), confirming its equilibrium and kinetic two-state unfolding behavior.

The chevron plots for Ubq–UIM also show a linear urea dependence of the folding and unfolding rate constants (Fig. 5). Fits of these plots to a two-state chevron model (Eq. (5)) yield very similar folding rate constants extrapolated to aqueous conditions (k_f) from CD ($k_{f,CD} = 10.3 \pm 0.3\ s^{-1}$) and fluorescence ($k_{f,FL} = 11.2 \pm 0.4\ s^{-1}$) experiments. Interestingly, this value is very similar to the k_f determined for Ubq from a global fit of CD and fluorescence experiments ($k_{f,CD/FL} = 10.9 \pm 0.5\ s^{-1}$). This agreement between $k_{f,CD}$ and $k_{f,FL}$ for Ubq–UIM, and $k_{f,CD/FL}$ for Ubq provides evidence that the UIM helix does not affect the folding rate of Ubq–UIM when monitored at the secondary and tertiary structure levels. In other words, the stability of the transition state ensemble (TSE) for Ubq–UIM folding is not influenced by the UIM helix. Furthermore, the folding rates of Ubq were not affected by the addition of the UIM peptide (see Fig. 5) again supporting the notion that likely the folding TSE for Ubq–UIM does not involve UIM helix. Additional support for this proposal comes from the observation that the kinetic m-values for folding (m_f), are the same for Ubq ($m_f = -3.4 \pm 0.2$ kJ mol^{-1} M^{-1}) and Ubq–UIM ($m_{f,CD} = -3.3 \pm 0.1$ kJ mol^{-1} M^{-1} and $m_{f,FL} = -3.4 \pm 0.1$ kJ mol^{-1} M^{-1}). Since m_f is proportional to the surface area buried in the TSE upon folding, a larger m_f value would be expected for Ubq–UIM than for Ubq if the UIM helix was docked to Ubq in the TSE.

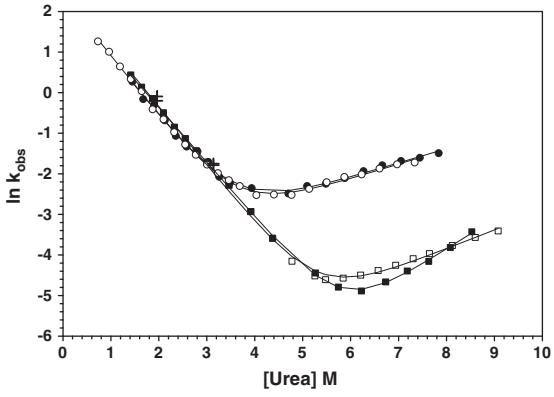

Fig. 5. Chevron plots showing the dependence of the kinetics of folding and unfolding of Ubq (circles) and Ubq–UIM (squares) on urea concentration, determined by stopped flow far-UV CD monitored at 222 nm (filled symbols) and fluorescence emission intensity collected with a 320 nm cutoff filter (open symbols). Solid lines represent fits of the data to a two-state chevron model (Eq. (5)) and the fitted parameters are listed in Table 2. Folding rates of 3 μM Ubq and 9 μM Ubq in the presence of 1.8 mM UIM peptide (crosses) were determined at final urea concentrations of 2 and 3 M.

Both CD and fluorescence experiments yield slower unfolding rates (k_u) for Ubq–UIM than for Ubq (Fig. 5 and Table 2). Considering the similarity in the folding rates, this observation suggests that the higher equilibrium stability of Ubq–UIM arises due to stabilization of its native state. This is expected since docking of the UIM helix would lower the free energy of the native state of Ubq–UIM by introducing stabilizing interactions at the Ubq/UIM interface. It is more interesting to note that for Ubq–UIM $k_{u,CD}$ is slower than $k_{u,FL}$ by almost an order of magnitude (Table 2), which translates to an apparent difference in stability $\Delta G^{H_2O}_{kin}$ of ~7 kJ/mol. This difference in unfolding rates accounts for the ~6 kJ/mol difference in $\Delta G^{H_2O}_{eq}$ from equilibrium unfolding of Ubq–UIM monitored by the two techniques. Moreover, analysis of CD data yields a larger kinetic m-value for unfolding ($m_{u,CD} = 1.9 \pm 0.2$ kJ mol^{-1} M^{-1}) than fluorescence ($m_{u,FL} = 0.9 \pm 0.1$ kJ mol^{-1} M^{-1}) (Table 2). The difference (~1 kJ mol^{-1} M^{-1}) is in good agreement with the difference in equilibrium m-values determined by these techniques (Table 1). It is also consistent with the estimates of changes in m-value of Ubq (4.0 kJ mol^{-1} M^{-1}) and Ubq–UIM (5.1 kJ mol^{-1} M^{-1}) based on the structural correlation (Eq. (7)). This suggests that smaller ΔASA for unfolding of Ubq–UIM is reported by the changes in the fluorescence intensity than by changes in the far-UV CD. Consequently, this provides additional support for the idea that fluorescence does not effectively monitor global unfolding of the Ubq–UIM protein but only of the Ubq domain, which in turn bolsters the argument that urea-induced unfolding of Ubq–UIM is not cooperative.

These conclusions on kinetics of folding/unfolding of the wild type Ubq–UIM are further supported by the results of kinetic analysis of folding/unfolding of three variants H77V_Ubq–UIM, R98V_Ubq–UIM, and E34N_Ubq–UIM (Table 2 and Fig. S1 in the Electronic Supplement). All these variants have the same folding rates and m_f-values as the corresponding Ubq core, suggesting the similarities in the transition state ensemble for folding. A major difference in stability of the variants comes from changes in the unfolding rate. Furthermore, there is excellent agreement between $\Delta G^{H_2O}_{eq}$ and $\Delta G^{H_2O}_{kin}$ for the variants as well (Table 1). Finally, the E43N_Ubq–UIM variant that shows the largest changes in the equilibrium cooperativity relative to the wild type Ubq–UIM also has the largest changes in the kinetic values, suggesting that unfolding of this variant is also very close to two-state.

3.4. Multi-state unfolding pathway for Ubq–UIM

We have previously established that the temperature-induced unfolding of Ubq–UIM follows a multi-state model [10]. Results presented above suggest that urea-induced unfolding as well as the kinetics of folding/unfolding of this protein is also not two-state, and allows further refinement of the model. The kinetic data are consistent with the free energy landscape presented in Fig. 3 and includes two intermediate states, the first occurs before the main rate-limiting step, and the second occurs after the main rate-limiting step. This model also rationalizes the apparent two-state chevron plots presented in Fig. 5. The intermediate I_{II} has partially folded UIM helix, and can be

Table 2
The folding/unfolding kinetic parameters for Ubq and Ubq–UIM variants.

Protein	Method	m_f (kJ mol^{-1}·M^{-1})	m_u (kJ mol^{-1}·M^{-1})	k_f (s^{-1})	k_u (s^{-1})
Ubq	CD&FL	-3.4 ± 0.2	0.7 ± 0.2	10.9 ± 0.5	$(1.4\pm0.1)\cdot10^{-2}$
Ubq–UIM	CD	-3.3 ± 0.1	1.9 ± 0.2	10.3 ± 0.3	$(5.0\pm0.1)\cdot10^{-5}$
	FL	-3.4 ± 0.1	0.9 ± 0.1	11.2 ± 0.4	$(5.2\pm0.9)\cdot10^{-4}$
H77V_Ubq	FL	-2.9 ± 0.1	1.2 ± 0.1	13.6 ± 0.4	$(7.9\pm1.0)\cdot10^{-3}$
H77V_Ubq–UIM	CD	-2.9 ± 0.1	2.0 ± 0.1	15.7 ± 0.5	$(1.1\pm0.7)\cdot10^{-5}$
	FL	-2.9 ± 0.1	1.2 ± 0.1	14.5 ± 0.4	$(1.4\pm0.3)\cdot10^{-4}$
E43N_Ubq	FL	-3.3 ± 0.1	0.9 ± 0.1	4.1 ± 0.2	$(6.9\pm0.5)\cdot10^{-2}$
E43N_Ubq–UIM	CD	-3.2 ± 0.2	1.9 ± 0.1	4.4 ± 0.8	$(3.3\pm0.8)\cdot10^{-4}$
	FL	-3.3 ± 0.1	1.7 ± 0.1	5.1 ± 0.4	$(5.9\pm0.8)\cdot10^{-4}$
R98V_Ubq–UIM	CD	-3.2 ± 0.1	1.8 ± 0.1	7.5 ± 0.7	$(7.1\pm0.9)\cdot10^{-4}$
	FL	-3.2 ± 0.1	1.5 ± 0.1	8.6 ± 0.9	$(1.4\pm0.4)\cdot10^{-3}$

The errors reported are from simultaneous fitting of the folding and unfolding data to the chevron equation (see Eq. (5) in Section 2).

observed only by CD. However, since helix folding is very fast [32,33], formation of I_{II} occurs within the dead-time of our experiments (i.e. occurs within first 2–3 ms). The intermediate I_I has partially folded UIM and fully folded Ubq domain, and is separated by a small barrier that leads to the formation of native Ubq–UIM. Folding of I_I to the native state is accompanied only by small changes in CD as it involves essentially folding and/or docking of UIM onto the Ubq domain. The rate-limiting step is defined by the folding of the Ubq domain and can be monitored by both CD and fluorescence. The observed folding rate of Ubq–UIM is defined by the height of the barrier between I_{II} and TSE (as the formation of I_{II} occurs within the experimental dead-time). This barrier is essentially the same as the barrier for Ubq folding as it manifests itself in similar values of k_f and m_f for Ubq and Ubq–UIM (see Table 2), and also rationalizes the linearity of the folding arm of chevron for Ubq–UIM.

The differences in the unfolding arm of the chevron plot can also be rationalized by a model presented in Fig. 3. The unfolding rates k_u for Ubq–UIM are much slower than for Ubq which suggests that the difference in stability is largely defined by the stability of the native state. The kinetic m_u-value for Ubq is very similar to that of Ubq–UIM when monitored by the fluorescence spectroscopy. Considering that N to I_I transition is not accompanied by the changes in fluorescence but only by CD, the $k_{u,FL}$ and correspondingly $m_{u,FL}$ report only on the unfolding of the Ubq domain of UIM. Accordingly, $m_{u,FL}$ of Ubq–UIM is similar to m_u of Ubq (0.9 ± 0.1 kJ mol^{-1} M^{-1} and 0.7 ± 0.1 kJ mol^{-1} M^{-1}, respectively, Table 2). CD reports on both N to I_I and I_I to TSE and consequently has different, albeit, slower $k_{u,CD}$ and higher $m_{u,CD}$. The observed single exponential relaxation and apparent linearity of the unfolding arm of the chevron plot is probably a consequence of two factors: 1) small amplitude of the changes in CD signal for $I_I \leftrightarrow N$ transition and 2) similarity in the relaxation rates for $N \rightarrow TSE_I$ and $I_I \rightarrow TSE$. It is important to note that the kinetic traces induced by small changes in urea concentrations produced the same rate constants suggesting that the two relaxations cannot be resolved in our experimental setup, and yet it appears that the observed rate constant includes both transitions as judged by the $m_{U,CD}$-value.

4. Concluding remarks

This study describes a fusion protein engineering approach to quantify the effect of stability of individual domains and inter-domain interactions on folding cooperativity in larger proteins, using the ubiquitin–UIM interaction system. Urea-induced unfolding profiles of the Ubq–UIM fusion protein exhibit a single sigmoidal transition as monitored at the secondary (far-UV CD at 222 nm) and tertiary (fluorescence spectroscopy) structure levels. Thermodynamic stabilities of Ubq–UIM are higher than the parent protein, Ubq, indicating that the UIM peptide is bound to Ubq in agreement with our previously solved NMR structure of the Ubq–UIM fusion protein. Kinetic folding studies show that Ubq and Ubq–UIM fold with similar rates suggesting that the UIM helix does not influence the stability of the transition state ensemble in Ubq–UIM folding. Kinetic unfolding experiments suggest that the higher stability of Ubq–UIM is due to a slower unfolding rate compared to Ubq. Most interestingly, comparison of equilibrium and kinetic stabilities of the fusion protein, as monitored by a single technique such as far-UV CD or fluorescence, failed to identify the deviation from a two-state unfolding behavior. However, comparison of the stability parameters determined from these two different experiments provided strong evidence of non two-state unfolding behavior in Ubq–UIM. Furthermore there is very good agreement between equilibrium and kinetic experimental data which further supports the non-cooperative unfolding behavior of Ubq–UIM.

The results on Ubq–UIM presented here together with the previous analysis of folding/unfolding cooperativity in repeat protein ankyrin [3–5], and two-domain protein spectrin [7–9], provide a strong thermodynamic foundation for the cooperativity model in proteins. The model for Ubq–UIM requires further refinement. One direction is to use an experimental setup that allows kinetic data collection on a much faster time scale and such experiments are currently in progress in the lab.

Finally, the Ubq–UIM model system provided a vivid example of how simple sigmoidal transition obtained by one spectroscopic method can be mistakenly assumed to be two-state. Thus, it is obvious that multiple spectroscopic probes are absolutely necessary for the analysis of protein cooperativity using denaturant induced unfolding.

Supplementary materials related to this article can be found online at doi:10.1016/j.bpc.2011.05.004.

Acknowledgments

This work was supported by a grant from NIH/NIGMSRO1-GM054537. We would like to thank Dr. Werner Streicher for the help with the stopped flow experiments. Instrumentation at the Core Facilities at the Center of Biotechnology and Interdisciplinary Studies at RPI were used for some of the experiments reported in this paper.

References

[1] J. Wyman, S. Gill, Binding and Linkage: Functional Chemistry of Biological Macromolecules, University Science Books, 1990.
[2] E. Di Cera, Thermodynamic Theory of Site-Specific Binding Processes in Biological Macromolecules, Cambridge University Press, 2005.
[3] E. Kloss, N. Courtemanche, D. Barrick, Repeat-protein folding: new insights into origins of cooperativity, stability, and topology, Archives of Biochemistry and Biophysics 469 (2008) 83–99.
[4] T.O. Street, C.M. Bradley, D. Barrick, Predicting coupling limits from an experimentally determined energy landscape, Proceedings of the National Academy of Sciences of the United States of America 104 (2007) 4907–4912.

[5] T. Aksel, A. Majumdar, D. Barrick, The contribution of entropy, enthalpy, and hydrophobic desolvation to cooperativity in repeat-protein folding, Structure 19 (2011) 349–360.
[6] I. Devries, D.U. Ferreiro, I.E. Sanchez, E.A. Komives, Folding kinetics of the cooperatively folded subdomain of the IkappaBalpha ankyrin repeat domain, Journal of Molecular Biology, 408 163–176.
[7] S. Batey, J. Clarke, Apparent cooperativity in the folding of multidomain proteins depends on the relative rates of folding of the constituent domains, Proceedings of the National Academy of Sciences of the United States of America 103 (2006) 18113–18118.
[8] S. Batey, L.G. Randles, A. Steward, J. Clarke, Cooperative folding in a multi-domain protein, Journal of Molecular Biology 349 (2005) 1045–1059.
[9] S. Batey, J. Clarke, The folding pathway of a single domain in a multidomain protein is not affected by its neighbouring domain, Journal of Molecular Biology 378 (2008) 297–301.
[10] M.M. Patel, N.G. Sgourakis, A.E. Garcia, G.I. Makhatadze, Experimental test of the thermodynamic model of protein cooperativity using temperature-induced unfolding of a Ubq–UIM fusion protein, Biochemistry 49 (2010) 8455–8467.
[11] N.G. Sgourakis, M.M. Patel, A.E. Garcia, G.I. Makhatadze, S.A. McCallum, Conformational dynamics and structural plasticity play critical roles in the ubiquitin recognition of a UIM domain, Journal of Molecular Biology 396 (2010) 1128–1144.
[12] C.N. Pace, F. Vajdos, L. Fee, G. Grimsley, T. Gray, How to measure and predict the molar absorption coefficient of a protein, Protein Science 4 (1995) 2411–2423.
[13] C.N. Pace, J.M. Scholtz, A helix propensity scale based on experimental studies of peptides and proteins, Biophysical Journal 75 (1998) 422–427.
[14] K.L. Shaw, J.M. Scholtz, C.N. Pace, G.R. Grimsley, Determining the conformational stability of a protein using urea denaturation curves, Methods in Molecular Biology (Clifton, N.J) 490 (2009) 41–55.
[15] W.E. Stites, M.P. Byrne, J. Aviv, M. Kaplan, P.M. Curtis, Instrumentation for automated determination of protein stability, Analytical Biochemistry 227 (1995) 112–122.
[16] C.N. Pace, Determination and analysis of urea and guanidine hydrochloride denaturation curves, Methods in Enzymology 131 (1986) 266–280.
[17] M.R. Hurle, G.A. Michelotti, M.M. Crisanti, C.R. Matthews, Characterization of a slow folding reaction for the alpha subunit of tryptophan synthase, Proteins 2 (1987) 54–63.
[18] A. Zarrine-Afsar, A.R. Davidson, The analysis of protein folding kinetic data produced in protein engineering experiments, Methods (San Diego, Calif.) 34 (2004) 41–50.
[19] K.L. Maxwell, D. Wildes, A. Zarrine-Afsar, M.A. De Los Rios, A.G. Brown, C.T. Friel, L. Hedberg, J.C. Horng, D. Bona, E.J. Miller, A. Vallee-Belisle, E.R. Main, F. Bemporad, L. Qiu, K. Teilum, N.D. Vu, A.M. Edwards, I. Ruczinski, F.M. Poulsen, B.B. Kragelund, S.W. Michnick, F. Chiti, Y. Bai, S.J. Hagen, L. Serrano, M. Oliveberg, D.P. Raleigh, P. Wittung-Stafshede, S.E. Radford, S.E. Jackson, T.R. Sosnick, S. Marqusee, A.R. Davidson, K.W. Plaxco, Protein folding: defining a “standard” set of experimental conditions and a preliminary kinetic data set of two-state proteins, Protein Science 14 (2005) 602–616.
[20] A. Ginsburg, W.R. Carroll, Some specific ion effects on the conformation and thermal stability of ribonuclease, Biochemistry 4 (1965) 2159–2174.
[21] C. Roumestand, M. Boyer, L. Guignard, P. Barthe, C.A. Royer, Characterization of the folding and unfolding reactions of a small beta-barrel protein of novel topology, the MTCP1 oncogene product P13, Journal of Molecular Biology 312 (2001) 247–259.
[22] A. Bachmann, T. Kiefhaber, Kinetic Mechanisms in Protein Folding, Wiley-VCH Verlag GmbH and Co., Weinheim, 2005.
[23] D.D. Banks, L.M. Gloss, Equilibrium folding of the core histones: the H3–H4 tetramer is less stable than the H2A–H2B dimer, Biochemistry 42 (2003) 6827–6839.
[24] S. Khorasanizadeh, I.D. Peters, T.R. Butt, H. Roder, Folding and stability of a tryptophan-containing mutant of ubiquitin, Biochemistry 32 (1993) 7054–7063.
[25] B.A. Krantz, T.R. Sosnick, Distinguishing between two-state and three-state models for ubiquitin folding, Biochemistry 39 (2000) 11696–11701.
[26] J.K. Myers, C.N. Pace, J.M. Scholtz, Denaturant m values and heat capacity changes: relation to changes in accessible surface areas of protein unfolding, Protein Science 4 (1995) 2138–2148.
[27] C.A. Rohl, R.L. Baldwin, Deciphering rules of helix stability in peptides, Methods in Enzymology 295 (1998) 1–26.
[28] J.M. Richardson, M.M. Lopez, G.I. Makhatadze, Enthalpy of helix–coil transition: missing link in rationalizing the thermodynamics of helix-forming propensities of the amino acid residues, Proceedings of the National Academy of Sciences of the United States of America 102 (2005) 1413–1418.
[29] G.I. Makhatadze, Thermodynamics of protein interactions with urea and guanidinium hydrochloride, The Journal of Physical Chemistry. B 103 (1999) 4781–4785.
[30] M. Auton, D.W. Bolen, Predicting the energetics of osmolyte-induced protein folding/unfolding, Proceedings of the National Academy of Sciences of the United States of America 102 (2005) 15065–15068.
[31] D.N. Ermolenko, S.T. Thomas, R. Aurora, A.M. Gronenborn, G.I. Makhatadze, Hydrophobic interactions at the Ccap position of the C-capping motif of alpha-helices, Journal of Molecular Biology 322 (2002) 123–135.
[32] S. Williams, T.P. Causgrove, R. Gilmanshin, K.S. Fang, R.H. Callender, W.H. Woodruff, R.B. Dyer, Fast events in protein folding: helix melting and formation in a small peptide, Biochemistry 35 (1996) 691–697.
[33] P.A. Thompson, W.A. Eaton, J. Hofrichter, Laser temperature jump study of the helix ⇔ coil kinetics of an alanine peptide interpreted with a ‘kinetic zipper’ model, Biochemistry 36 (1997) 9200–9210.
[34] W. Humphrey, A. Dalke, K. Schulten, VMD: visual molecular dynamics, Journal of Molecular Graphics 14 (1996) 33–38 http://www.ks.uiuc.edu/Research/vmd/ 27–38.